Low-energy resonances in $^{14}N(\alpha,\gamma)^{18}F$ and their astrophysical implications

J. Görres,[1,2] C. Arlandini,[2] U. Giesen,[1] M. Heil,[2] F. Käppeler,[2] H. Leiste,[3] E. Stech,[1] and M. Wiescher[1]
[1]*Department of Physics, University of Notre Dame, Notre Dame, Indiana 46556*
[2]*Forschungszentrum Karlsruhe, Institut für Kernphysik, Karlsruhe, Germany*
[3]*Forschungszentrum Karlsruhe, Institut für Materialforschung I, Karlsruhe, Germany*
(Received 31 May 2000; published 3 October 2000)

The strengths of low-energy resonances in $^{14}N(\alpha,\gamma)^{18}F$ at 573 keV and 1136 keV have been measured using an activation method. In addition, their relative strength and the energy of the lower resonance have been determined in a prompt γ-ray experiment. The results of these measurements are used to reevaluate the stellar reaction rate of $^{14}N(\alpha,\gamma)^{18}F$. The present reaction rate at temperatures of astrophysical interest is a factor of 2 smaller than previously reported.

PACS number(s): 26.20.+f, 25.55.−e, 25.70.Ef

I. INTRODUCTION

Stellar He burning is the dominant energy source during the red giant phase of stellar evolution. The energy generation is determined by the triple α reaction and the subsequent $^{12}C(\alpha,\gamma)^{16}O$ with the helium being produced in the preceding hydrogen burning phase [1]. In massive stars hydrogen burning is dominated by the CNO cycles which not only fusion catalytically hydrogen to helium but also convert the initial ^{12}C and ^{16}O abundances to ^{14}N [2]. The ^{14}N abundances provide one of the neutron sources for *s*-process nucleosynthesis in massive stars. During stellar He burning ^{14}N is converted via the $^{14}N(\alpha,\gamma)^{18}F(\beta,\nu)^{18}O$ reaction sequence to ^{18}O, further alpha capture reactions $^{18}O(\alpha,\gamma)^{22}Ne$ produce ^{22}Ne which has been identified as one of the main neutron sources, $^{22}Ne(\alpha,n)$ [3–5]. Due to the negative Q value of the $^{22}Ne(\alpha,n)$ reaction, neutrons are not released during the relatively cool He burning phase but only towards the end of He burning when due to He depletion the energy generation decreases, and the core starts to contract gravitationally. This leads to an increase in core temperature and pressure which ignites the $^{22}Ne(\alpha,n)^{25}Mg$ reaction [4,5]. This reaction is considered to be the main neutron source for the weak component of the *s* process which is responsible for the nucleosynthesis of the light *s*-process nuclei in the mass range of $A=60-90$ [4,5]. The development of temperature and density conditions during the He burning phase of a 13, 15, and 20 $M_\odot$ star is shown in Fig. 1. The details of the model are described in Ref. [6]. Figure 2 shows the main reaction branches during the He-burning phase. For a reliable interpretation of the *s*-process nucleosynthesis during the late phase the preceding processing of ^{14}N and ^{18}O needs to be understood to obtain the ignition abundance of ^{22}Ne and the subsequent development of the neutron flux. This requires a detailed study of both $^{14}N(\alpha,\gamma)^{18}F$ and $^{18}O(\alpha,\gamma)^{22}Ne$ reactions in the stellar energy range. In both cases the reaction rate at stellar temperatures is determined by low energy resonances which need to be studied in detail.

The reaction rate of the $^{14}N(\alpha,\gamma)^{18}F$ reaction is dominated by the contribution of a $J^\pi=1^-$ resonance at an α energy of 572 keV[1] for temperatures of astrophysical interest, $T=0.1-0.5$ GK. For higher temperatures the contributions of resonances at higher energies ($E_R=1136$ keV, 1398 keV, 1527 keV, 1529 keV, and 1618 keV) become more important. Below 0.1 GK additional contributions are possible from the low-energy tail of the 572 keV resonance, the direct capture (DC), and the $J^\pi=4^+$, $T=1$ resonance at 305 keV. All other contributions can be neglected [7–9].

The lowest known resonance is the $J^\pi=1^-$ resonance at 572 keV. The strengths of this resonance and the resonance at 1136 keV were measured by Couch *et al.* [7] using an activation method and thick TiN targets in which the α beam was stopped. The energy step size in this experiment was too large ($\Delta E \geqslant 60$ keV) for a meaningful determination of the resonance energy. They identified the resonance as the $E_x=4849$ keV, $J=1$ state in ^{18}F, which was the only state known at the time [10] in the relevant energy window (500–600 keV) and deduced a resonance energy of 559 keV. This resonance energy has been used in all previous calculations of the reaction rate [7–9]. More recent results locate the state at $E_x=4860$ keV [11] resulting in a resonance energy of 572 keV. The strength of the 1136 keV resonance was independently measured by Parker [12] also using thick TiN targets and an activation method. Before comparing the results for the 1136 keV resonance the values have to be renormalized to the same set of stopping powers. The stopping power of Ziegler [13] was adopted and a correction of 14/18 was applied to both values to derive the center-of-mass resonance strength. The results of this renormalization are shown in Table I and reveal that the strength of Couch *et al.* [7] is approximately 50% larger than the value of Parker [12]. The recent NACRE compilation [9] adopted the renormalization of Rolfs *et al.* [14] leading to slight differences to the present values (see Table I).

To investigate this discrepancy we have measured the strength of both resonances using an activation method. In addition we applied the prompt γ-ray technique to measure the relative strength of both resonances and to measure the

[1]All α energies are given in the laboratory system.

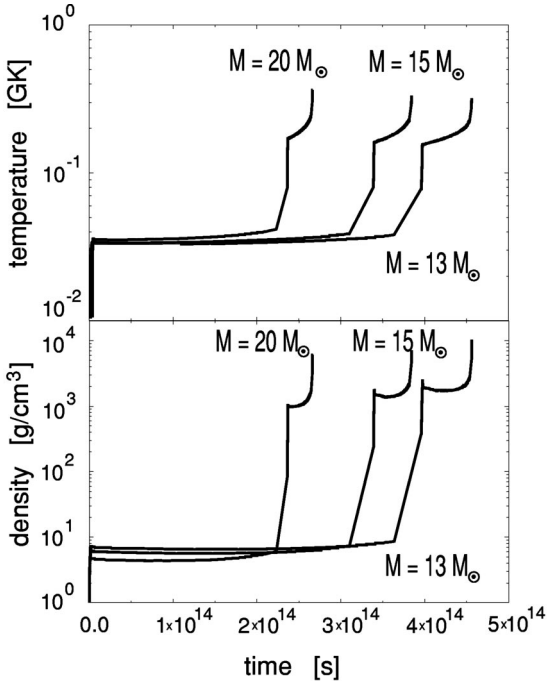

FIG. 1. Temperature (upper panel) and density (lower panel) development for three massive star models, $M=13$, 15, 20 $M_{\odot}$. The development is calculated from the beginning of the hydrogen burning phase to the end of the helium burning phase. (Courtesy of Alessandro Chieffi.)

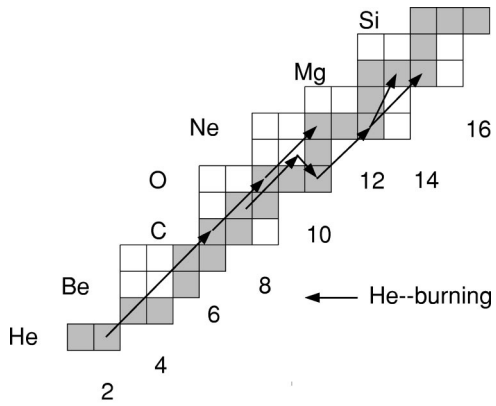

FIG. 2. The reaction flow during stellar helium burning. The reaction sequence $^{4}\mathrm{He}(2\,^{4}\mathrm{He},\gamma)^{12}\mathrm{C}(\alpha,\gamma)^{16}\mathrm{O}$ is responsible for the energy generation; the reaction sequence $^{14}\mathrm{N}(\alpha,\gamma)^{18}\mathrm{F}(\beta^{+}\nu)^{18}\mathrm{O}(\alpha,\gamma)^{22}\mathrm{Ne}(\alpha,n)$ represents the neutron source for the weak *s*-process component.

resonance energy of the lowest resonance for the first time. The following sections describe the experimental setup and the experimental results. In the final section we present a reevaluation of the stellar reaction rate of $^{14}\mathrm{N}(\alpha,\gamma)^{18}\mathrm{F}$.

II. EXPERIMENTAL SETUP

The experiment was performed at the KN accelerators at the Institut für Kernphysik of the Forschungszentrum Karlsruhe and at the Nuclear Structure Laboratory at the University of Notre Dame in an energy range of 550 keV to 1300 keV with α-beam currents of $50-100$ μA. The beam energy was calibrated to ± 2 keV using the well known $^{27}\mathrm{Al}(p,\gamma)^{28}\mathrm{Si}$ resonances at 632 keV and 992 keV [15], the observed γ-ray energies of primary DC transitions in the reaction $^{16}\mathrm{O}(p,\gamma)^{17}\mathrm{F}$ [16] at several energies over the energy range of the experiment, and the $^{14}\mathrm{N}(\alpha,\gamma)^{18}\mathrm{F}$ resonance at 1136 ± 3 keV [11]. Targets were directly water cooled and mounted at 45° with respect to the beam direction. The position of the beam was defined by a set of horizontal slits and a collimator. The beam was swept horizontally and vertically across an effective target area of 1 cm^2 by steerers to illuminate the target homogeneously. A liquid nitrogen cooled copper tube was placed between the collimator and the target to minimize carbon deposits. Target and chamber formed the Faraday cup and a negative voltage (-300 V) was applied to the Cu tube to suppress secondary electron emission.

The nitrogen targets consisted of a thin layer of TiN on a 0.25 mm thick Ta backing. For the relative measurement of the resonance strengths layers of TiN ($20-40$ μg/cm^2) were prepared by evaporating Ti onto the Ta backing and then heating the target in a pure nitrogen atmosphere to about 800 °C [14]. For the activation measurements TiN targets were prepared by sputtering of TiN onto the Ta backings. This procedure is well studied because of the technical applications, e.g., in the hardening of tools. Tests have shown that deviations from the stoichiometry of Ti:N=1:1 are $\leqslant 2\%$. The targets had a thickness of 30 μg/cm^2 which

TABLE I. Yield and resonance strength $\omega\gamma$ of low-energy resonances in $^{14}\mathrm{N}(\alpha,\gamma)^{18}\mathrm{F}$. The errors of the $\omega\gamma$ values do not include a common uncertainty of the stopping power (7%).

E_R [keV]	Yield [^{18}F/($10^{15}\alpha$'s)] present	Resonance strength $\omega\gamma$ [meV] present	[meV] [12] [a]	[meV] [7] [a]	[meV] [9] [b]	[meV] adopted [c]
573 ± 3 [d]	1.26 ± 0.07	$(45\pm 3)\times 10^{-3}$		$(96\pm 14)\times 10^{-3}$	$(6\pm 1)\times 10^{-2}$	$(46\pm 3)\times 10^{-3}$
1136 ± 3 [e]	323 ± 4	21.0 ± 0.3	22.4 ± 1.0	35.1 ± 3.2	24 ± 1	21.1 ± 0.3

[a] Renormalized; for details see text.
[b] Adopted by NACRE [9]; see text.
[c] See text.
[d] Adopted value (see text).
[e] From [11].

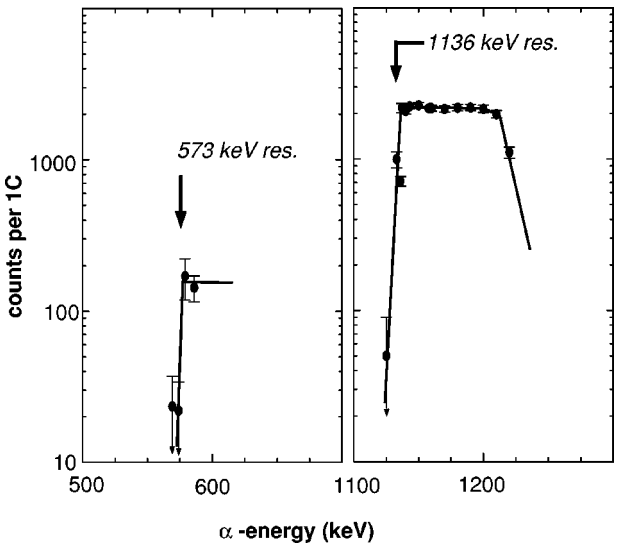

FIG. 3. Yield of the 1042 keV γ-ray transition at the 573 keV resonance (left panel) and the yield of the 2523 keV γ-ray transition at the 1136 keV resonance (right panel) (for more details see text).

corresponds to an α energy loss of 46 keV at an energy of 600 keV. The targets proved to be extremely stable under the bombardment with a low-energy α beam. The target stability has been verified repeatedly during the course of the experiment by measuring the strong $^{14}N(p,\gamma)^{15}O$ resonance at 1058 keV [17] before and after measurements with α beams. No noticeable change in the reaction yield and thus in stoichiometry has been observed even after an accumulated charge of 11 C. In addition, Couch *et al.* [7] have shown that no ^{18}F activity produced in the target is lost during the bombardment of the target with α beams. This last point is of special importance for the activation measurements.

Prompt reaction γ rays were detected with a Ge-clover detector in close geometry at 45° with respect to the beam. The Ge-clover detector consisted of four individual crystals each with a relative efficiency of 20% and was shielded by 10 cm of Pb to reduce the γ-ray room background. The large angle opening of the clover detector would lead to a large Doppler broadening of the γ lines. In order to minimize this broadening the clover detector was subdivided electronically into two pairs of crystals with both crystals of a pair at the same reaction angle. The relative efficiency was determined from the known γ decay of the $^{14}N(p,\gamma)^{15}O$ resonance at 1058 keV, of the $^{14}N(\alpha,\gamma)^{18}F$ resonance at 1136 keV, as well as by calibrated γ sources.

During the activation experiment the ^{18}F activity was measured by counting the 511 keV annihilation γ rays in coincidence. The detection system consisted of two Ge clover detectors mounted face to face. The detectors were shielded by 5 cm of Pb against room background and the distance between the front surfaces of the two detectors was 5 mm. The activated targets were mounted in a holder which placed them at the center of the detection system. The holder was made out of plastic and filled out the whole volume between the clover detectors except for the space needed for the target. The absolute counting efficiency was measured with a weak ^{22}Na source mounted on a Ta backing of the same thickness as the targets. The efficiency is given independently of the source strength by the ratio of the triple coincidence rate (511:511:1274 keV) and the single rate of the 1274 keV γ line corrected for the 10.8% decay via electron capture [15]. For a point source an absolute counting efficiency of $\epsilon_\gamma=(3.457\pm0.012)\%$ was found. This efficiency has to be corrected for the fact that the ^{18}F activity produced during the activations is distributed over the entire irradiated area of 1 cm^2. Monte Carlo simulations of the counting efficiency for a point source and for a extended source using the computer code GEANT [18] were performed resulting in a correction factor of 0.961. The background rate of the counting system was (0.58 ± 0.07)/h.

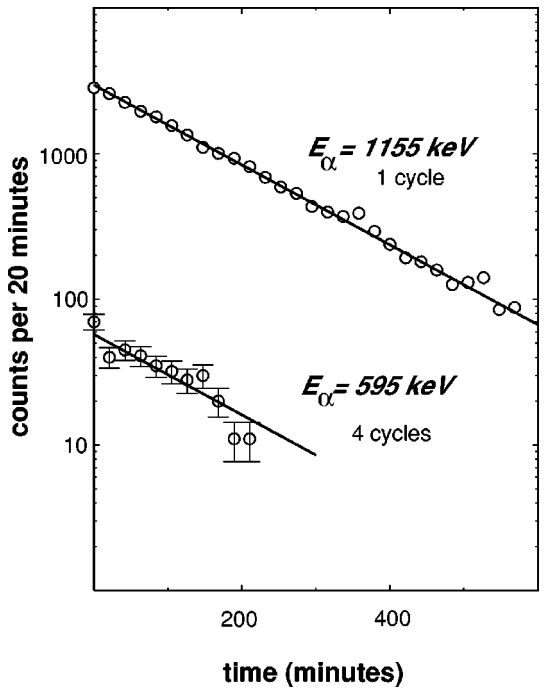

FIG. 4. Decay curves obtained for the two resonances at 573 keV and 1136 keV. The solid lines represent fits to the decay curve (for more details see text).

III. EXPERIMENTAL RESULT

In a first step we have measured the energy of the lowest known resonance in the reaction $^{14}N(\alpha,\gamma)^{18}F$ and its strength relative to the resonance at 1136 keV using prompt γ-ray spectroscopy. The energy has been listed as 559 keV in the latest compilations [9,11]. However, this energy has not been measured directly but had been deduced from the excitation energy of the $J^\pi=1^-$ state at 4849 keV and the reaction Q value [7]. More recent information on the excitation energy ($E_x=(4860\pm2)$ keV [11]) and Q value ($Q=(4414.9\pm0.6)$ keV [19]) lead to a revised value of the resonance energy of (572 ± 2.7) keV. To verify this resonance energy we have measured an excitation function across the expected resonance energy in 5 keV steps. Figure 3 shows the yield of the isotropic 1042 keV γ line from the ground state decay of the $J^\pi=0^+$ state at 1042 keV. This secondary γ transition represents $(66\pm11)\%$ of all γ decays

TABLE II. Stellar reaction rate for the $^{14}N(\alpha,\gamma)^{18}F$ reaction.

Temperature [GK]	$N_A\langle\sigma v\rangle_{DC}$ present	$N_A\langle\sigma v\rangle_{305}$ present	$N_A\langle\sigma v\rangle_{expt}$ present [cm^3/(s mole)]	$N_A\langle\sigma v\rangle_{CF88}$ [8]	$N_A\langle\sigma v\rangle_{NACRE}$ [9]
0.0700	7.08×10^{-29}	3.24×10^{-28}	5.66×10^{-31}	5.64×10^{-26}	1.05×10^{-26}
0.0800	2.91×10^{-27}	3.60×10^{-26}	4.76×10^{-27}	6.80×10^{-24}	1.19×10^{-24}
0.0900	6.73×10^{-26}	1.38×10^{-24}	5.25×10^{-24}	3.07×10^{-22}	7.27×10^{-23}
0.1000	1.00×10^{-24}	2.51×10^{-23}	1.41×10^{-21}	1.25×10^{-20}	7.37×10^{-21}
0.1500	1.40×10^{-20}	1.32×10^{-19}	2.35×10^{-14}	8.14×10^{-14}	7.18×10^{-14}
0.2000	5.68×10^{-18}	8.43×10^{-18}	8.47×10^{-11}	2.41×10^{-10}	2.09×10^{-10}
0.3000	1.05×10^{-14}	4.50×10^{-16}	2.56×10^{-7}	5.96×10^{-7}	5.10×10^{-7}
0.4000	1.18×10^{-12}	2.90×10^{-15}	1.24×10^{-5}	2.61×10^{-5}	2.22×10^{-5}
0.5000	3.39×10^{-11}	8.22×10^{-15}	1.20×10^{-4}	2.34×10^{-4}	2.00×10^{-4}
0.6000	4.36×10^{-10}	1.57×10^{-14}	5.58×10^{-4}	9.79×10^{-4}	8.73×10^{-4}
0.7000	3.34×10^{-9}	2.39×10^{-14}	1.98×10^{-3}	2.87×10^{-3}	2.83×10^{-3}
0.8000	1.79×10^{-8}	3.21×10^{-14}	6.81×10^{-3}	7.89×10^{-3}	8.75×10^{-3}
0.9000	7.37×10^{-8}	3.93×10^{-14}	2.27×10^{-2}	2.28×10^{-2}	2.71×10^{-2}
1.0000	2.49×10^{-7}	4.56×10^{-14}	6.82×10^{-2}	6.48×10^{-2}	7.81×10^{-2}
1.5000	1.80×10^{-5}	6.21×10^{-14}	2.59×10^{0}	2.43×10^{0}	2.90×10^{0}
2.0000	2.65×10^{-4}	6.39×10^{-14}	1.59×10^{1}	1.54×10^{1}	1.84×10^{1}
3.0000	7.50×10^{-3}	5.49×10^{-14}	9.07×10^{1}	9.14×10^{1}	1.05×10^{2}
4.0000	6.08×10^{-2}	4.50×10^{-14}	2.39×10^{2}	2.10×10^{2}	2.77×10^{2}
5.0000	2.66×10^{-1}	3.69×10^{-14}	4.58×10^{2}	3.35×10^{2}	5.30×10^{2}
6.0000	8.17×10^{-1}	3.00×10^{-14}	7.42×10^{2}	4.48×10^{2}	8.59×10^{2}
7.0000	1.99×10^{0}	2.61×10^{-14}	1.10×10^{3}	5.42×10^{2}	1.27×10^{3}
8.0000	4.13×10^{0}	2.24×10^{-14}	1.53×10^{3}	6.17×10^{2}	1.77×10^{3}
9.0000	7.64×10^{0}	1.95×10^{-14}	2.04×10^{3}	6.77×10^{2}	2.36×10^{3}
10.0000	1.30×10^{0}	1.72×10^{-14}	2.65×10^{3}	7.23×10^{2}	3.07×10^{3}

of the 4849 keV state [11]. The excitation function shows a resonance at (577.5 ± 4.5) keV. The error is the sum of the uncertainty due to the step size (±2.5 keV) and the error of the beam energy calibration (±2 keV). This is in very good agreement with the previous result and we adopt a resonance energy of $(573\pm3$ keV).

The excitation function across the 1136 keV resonance is also shown in Fig. 3. For this resonance the yield of the strong 2523 keV γ transition is shown normalized to the on resonance yield of the 1042 keV transition. Correcting the observed count rates with the corresponding decay branching ratios [11] results in a reaction yield ratio of the two resonances of Y(1136 keV)/Y(573 keV) $=275\pm77$. This is in good agreement with the ratio derived from the results of Couch *et al.* [7], 200 ± 35. The large error of the present result is equally caused by the statistical error and the uncertainties of the branching ratios [11].

In a second step, the resonance strengths of the resonances at 573 keV and 1136 keV have been measured in an activation experiment. The reaction product, ^{18}F, has a half life of (109.77 ± 0.05) minutes and decays to $(96.73\pm0.04)\%$ by β^+ decay producing two 511 keV γ rays [11]. For this reason the reaction $^{14}N(\alpha,\gamma)^{18}F$ is well suited for an activation experiment. The advantage of this method is the large sensitivity (see Sec. II) and the fact that the determination of the resonance strength does not depend on the γ-branching ratios of the resonance and their uncertainties, but only on the well-known decay properties of ^{18}F. At these low α energies no other reaction channel leading to the formation of ^{18}F is open [7,11].

In the present experiments the targets were activated for 220 min (two half-lifes). After the activation the targets were removed from the target chamber and transferred to the counting station (see Sec. II), where the decay curves were measured for at least two half-lives. For the measurements of the resonance strengths α energies of about 20 keV (half the target thickness) above the resonance energies were chosen. During the activations the beam current was recorded as a function of time to correct the produced activities for fluctuations of the beam intensities which were constant within $\leqslant10\%$. Figure 4 shows the decay curves for the resonances at 573 keV and 1136 keV. The data for the lower resonance is the sum of four individual activations. Additional activations were carried out (1) at an energy below the 573 keV resonance and (2) with an Al target of similar thickness at the same energy as the activation runs for the 573 keV resonance. No activity in excess of the background rate (see Sec. II) was observed in both cases.

The resulting resonance yields are presented in column 2 of Table I. The quoted errors include the statistical uncertainty and the errors of the detection efficiency (0.35%) and the charge integration (1%). The resonance strength $\omega\gamma$ is defined by

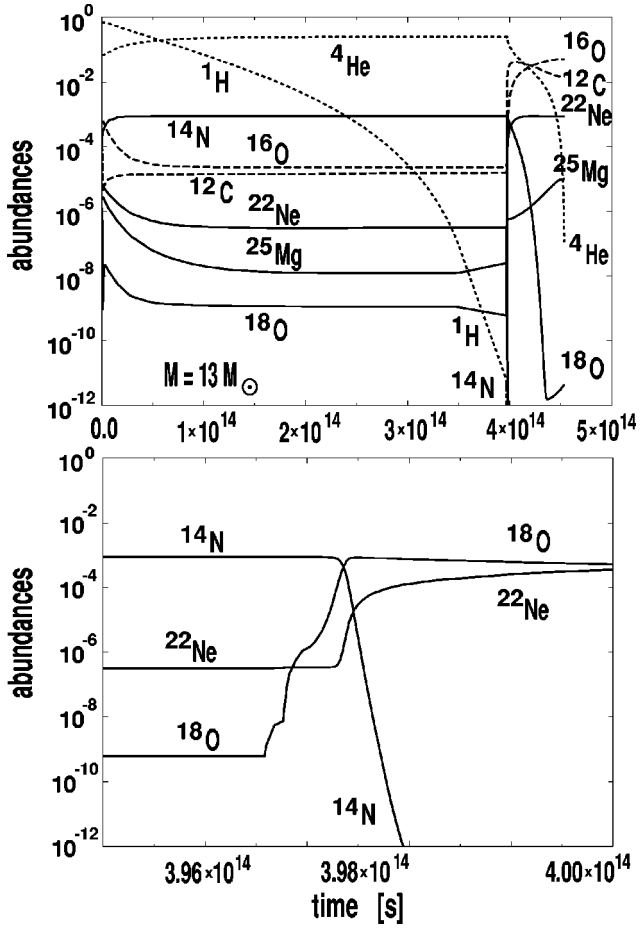

FIG. 5. The upper panel shows the development of the isotopic abundances of ^{1}H and ^{4}He (dotted lines), ^{12}C and ^{16}O (dashed lines), and ^{14}N, ^{18}O, ^{22}Ne, and ^{25}Mg during the hydrogen and helium burning phase of a $M=13\ M_{\odot}$ star (see Fig. 1). The lower panel shows the rapid depletion of ^{14}N into ^{18}O and subsequently into ^{22}Ne during the contraction phase of the core of the main sequence star and the ignition of helium burning.

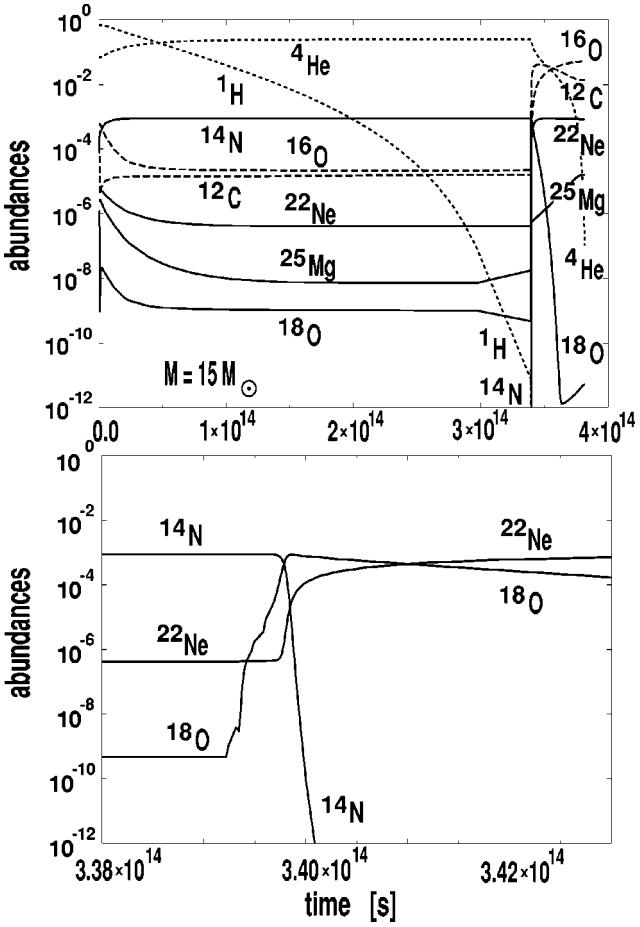

FIG. 6. The upper panel shows the development of the isotopic abundances of ^{1}H and ^{4}He (dotted lines), ^{12}C and ^{16}O (dashed lines), and ^{14}N, ^{18}O, ^{22}Ne, and ^{25}Mg during the hydrogen and helium burning phase burning phase of a $M=15\ M_{\odot}$ star (see Fig. 1). The lower panel shows the rapid depletion of ^{14}N into ^{18}O and subsequently into ^{22}Ne during the contraction phase of the core of the main sequence star and the ignition of helium burning.

$$\omega\gamma = \frac{2J_R+1}{(2j_p+1)(2j_t+1)}\frac{\Gamma_\alpha\Gamma_\gamma}{\Gamma}, \tag{1}$$

with J_R (j_p,j_t) the spin of the resonance (projectile,target) and Γ $(\Gamma_\alpha,\Gamma\gamma)$ the total (α,γ) width of the resonance. It can be calculated from the reaction yield Y_R according to

$$\omega\gamma = \frac{m_p}{(m_p+m_t)}\frac{2\epsilon}{\lambda^2}Y_R, \tag{2}$$

with m_p (m_t) the mass of the projectile (target), ϵ the stopping power [13], and λ the center-of mass De Broglie wave length at the resonance energy. The results are shown in Table I together with the resonance strengths of Parker [12] and Couch *et al.* [7]. For the 1136 keV resonance the present resonance strength is in excellent agreement with the value of Parker [12]. We have adopted the weighted average of (21.3 ± 0.3) meV. In contrast the present strengths for both resonances are about 40% smaller than those of Couch *et al.* [7]. However, the relative resonance yield of Couch *et al.* [7], 200 ± 35, is within the errors in good agreement with the present values from the prompt and the activation method, 275 ± 77 and 256 ± 15, respectively. The adopted strength of (46 ± 3) μeV for the 573 keV resonance is the weighted average of the present absolute measurement and the relative measurements. The errors of the resonance strengths quoted in Table I do not include the uncertainty in the stopping power, because all values have been calculated using the stopping powers of Ziegler [13]. From the relevant figures in Ref. [13] we estimate an uncertainty of 7% for the stopping power for TiN at the α energies of interest. This common error has to be added to the uncertainties given in Table I.

IV. STELLAR REACTION RATE AND ASTROPHYSICAL IMPLICATIONS

The contributions of resonances to the reaction rate of $^{14}N(\alpha,\gamma)^{18}F$ is given by

$$N_A\langle\sigma v\rangle_{\rm res} = 2.81\times10^4 T_9^{-3/2}\omega\gamma e^{-11.605E_{\rm c.m.}/T_9}, \tag{3}$$

with T_9 the temperature in GK, $\omega\gamma$ the resonance strength in eV, and $E_{\text{c.m.}}$ the center-of-mass resonance energy in MeV. We have calculated the experimentally determined reaction rate from the strengths of the two resonances studied in this experiment and the contribution of additional resonances at 1398 keV, 1527/9 keV, and 1618 keV [11]. For these resonances we adopted the resonance strengths of Parker [12] normalized to the present strength of the 1136 keV resonance. For temperatures above 2 GK the number of contributing resonances increases rapidly with temperature. For this reason we have adopted the Hauser-Feshbach rate of the NACRE compilation [9] for $T \geqslant 2$ GK normalized to the experimental rate at $T=2$ GK. The resulting reaction rate $N_A\langle\sigma v\rangle_{\text{expt}}$ is listed in Table II as a function of the temperature. For $T \leqslant 0.7$ GK this rate is completely dominated by the contribution of the lowest resonance at 573 keV.

At low temperatures possible contributions could arise from the nonresonant DC, the low-energy tail of the 573 keV resonance and the $J=4^+, T=1$ resonance at 305 keV [7]. We have calculated the cross section of the direct capture to the low lying states in ^{18}F assuming a spectroscopic factor of 0.1. The resulting S factor $S(0)=0.085$ MeV b is in good agreement with the previous value of 0.1 MeV b [7]. The reaction rate is given by

$$N_A\langle\sigma v\rangle_{\text{DC}} = 1.01\times 10^9 T_9^{-2/3} e^{-36.023 T_9^{-1/3}}, \qquad (4)$$

and also listed in Table II. The contribution of the low-energy tail of the 573 keV resonance has been previously calculated using a total width of $\Gamma=1$ eV [7]. In a later experiment the lifetime of this state has been measured [20] leading to a width of 10 meV. This reduces the reaction rate by about two orders of magnitude and its contribution to the total rate is now small compared to that of the direct capture. The first $J=4^+, T=1$ state is located at an α energy of 305 keV. The resonance energy was derived from the excitation energy of $E_x=4652$ keV [11] and a Q value of 4414.9 keV. Its analogue in ^{18}O is the 4^+ state at 3555 keV which has a known α-spectroscopic factor of $S_\alpha=0.03$ [21]. However, the formation of this state is isospin forbidden in the ^{14}N $+\alpha$ channel. Based on experiments and theoretical investigations of $T=1/2$ impurities in $T=3/2$ states [22] and of $T=1$ admixtures in $T=0$ ground states [23] a suppression factor of $f_{\text{iso}} = \approx 10^{-3}$ has been estimated for this state. The α width of the state is given by

$$\Gamma_\alpha = S_\alpha f_{\text{iso}} \Gamma_\alpha^{\text{sp}}. \qquad (5)$$

The single particle width $\Gamma_\alpha^{\text{sp}} = 2.85\times 10^{-13}$ eV has been calculated in a Woods-Saxon potential with a radius of $R=3.01$ fm and a diffuseness of $a=0.65$ fm. This results in a resonance strength of $\omega\gamma \approx 3\Gamma_\alpha = 2.6\times 10^{-17}$ eV. The present result is about a factor of 300 smaller than the estimate of Couch *et al.* [7]. There are two reasons for this change: (1) the more realistic calculation of $\Gamma_\alpha^{\text{sp}}$ leads to a reduction by a factor of 10, and (2) Couch *et al.* [7] chose $S_\alpha \cdot f_{\text{iso}} = 10^{-3}$ as a conservative upper limit. The present reaction rate of the 305 keV resonance is listed in Table II. It should be noted that this resonance contributes significantly to the reaction only for temperatures below $T=0.1$ GK even with a considerably larger isospin mixing than presently assumed.

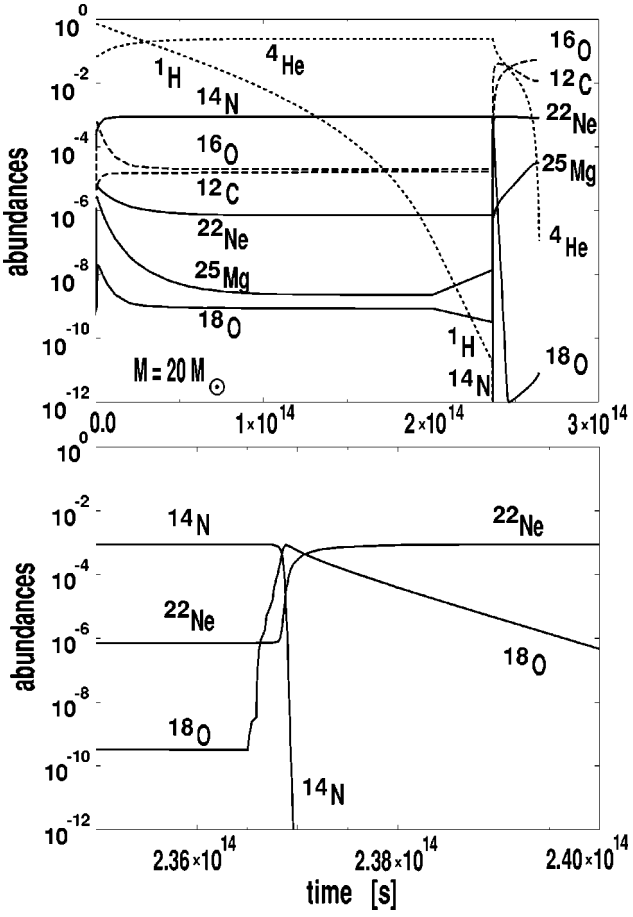

FIG. 7. The upper panel shows the development of the isotopic abundances of ^{1}H and ^{4}He (dotted lines), ^{12}C and ^{16}O (dashed lines), and ^{14}N, ^{18}O, ^{22}Ne, and ^{25}Mg during the hydrogen and helium phase of a $M=20\ M_\odot$ star (see Fig. 1). The lower panel shows the rapid depletion of ^{14}N into ^{18}O and subsequently into ^{22}Ne during the contraction phase of the core of the main sequence star and the ignition of helium burning.

For comparison, we have listed the reaction rate of Caughlan and Fowler [8] and NACRE [9]. The present reaction rate is a factor of 2–5 smaller than the previous rates in astrophysical important temperature range of $T=0.1-0.5$ GK. This change results mainly from the revised energy of the lowest known resonance from 559 keV to the present value of 573 keV.

To investigate the development of the ^{14}N abundances and the subsequent production of ^{18}O and ^{22}Ne network calculations have been performed in post-processing mode within the framework of a 1-zone model for the temperature and density development of a 13, 15, and 20 $M_\odot$ star shown in Fig. 1 [6]. The calculations followed the hydrogen and helium burning phase and were performed with an initial solar abundance distribution [24]. Figures 5–7 show the development of the isotopic abundances of ^{14}N, ^{18}O, ^{22}Ne, and ^{25}Mg during the initial hydrogen burning phase and the helium burning phase of these stars. Also shown are the iso-

topic abundances of ^{1}H and ^{4}He as well as of ^{12}C and ^{16}O to monitor the development of these abundances. It can be clearly seen that after exhaustion of hydrogen burning the increasing density and temperature due to core contraction (see Fig. 1) initiates the helium burning phase after $(3-4)\times10^{14}$ s, depending on the mass of the star. The helium burning causes rapid depletion of the ^{14}N abundance generated during the preceding CNO burning. The lower panels of Figs. 5–7 focus on the ^{14}N nucleosynthesis during the core contraction phase. They show that already within less than 10^{5} years after the ignition of the helium burning phase ^{14}N is completely converted to ^{18}O due to its relatively large reaction rate. The ^{18}O abundance is more slowly converted to ^{22}Ne due to the smaller reaction rate for $^{18}O(\alpha,\gamma)^{22}Ne$ [5]. This reaction rate, however, still carries considerable uncertainties associated with possible low-energy resonances [25]. Further experimental work is necessary to remove these uncertainties. Towards the end of the helium burning phase the abundance of ^{22}Ne is still high for all three cases. Only the rapid increase of temperature towards the end of the helium burning phase allows an efficient operation of the $^{22}Ne(\alpha,n)$ neutron source. The rapid decline of the helium fuel on the other side puts severe limits on the neutron production. An expansion of the helium burning zone plus rapid mixing of fresh helium material into the core region towards the end of the helium burning phase may enhance neutron production. These processes also bring unprocessed ^{14}N into the burning zone which will be rapidly converted to ^{22}Ne causing a further increase of the neutron flux. A more quantitative consideration is, however, beyond the range of this model.

ACKNOWLEDGMENTS

We like to thank the technical staffs at Karlsruhe and Notre Dame for their excellent support. We thank Alessandro Chieffi for making the temperature and density profiles for massive stars available to us. This work was supported by the National Science Foundation Grants No. PHY98-03575 and No. INT98-15296 and by the Deutscher Akademischer Austauschdienst Grant No. DAAD 315/PPP/ab. We would also like to acknowledge financial support by the Graduate School of the University of Notre Dame.

[1] C. Rolfs and W. Rodney, *Cauldrons in the Cosmos* (University of Chicago Press, Chicago, 1988).
[2] M. Wiescher, J. Görres, and H. Schatz, J. Phys. G **25**, R133 (1999).
[3] A.G.W. Cameron, Astrophys. J. **121**, 144 (1955); Astron. J. **65**, 485 (1960).
[4] C.M. Raiteri, M. Busso, R. Gallino, G. Picchio, and L. Pulone, Astrophys. J. **367**, 228 (1991).
[5] F. Käppeler, M. Wiescher, U. Giesen, J. Görres, I. Baraffe, M. El Eid, C.M. Raiteri, M. Busso, R. Gallino, M. Limongi, and A. Chieffi, Astrophys. J. **437**, 396 (1994).
[6] A. Chieffi, M. Limongi, and O. Straniero, Astrophys. J. **502**, 737 (1998).
[7] R.G. Couch, H. Spinka, T.A. Tombrello, and T.A. Weaver, Nucl. Phys. **A175**, 300 (1971).
[8] G.R. Caughlan and W.A. Fowler, At. Data Nucl. Data Tables **40**, 283 (1988).
[9] C. Angulo *et al.*, Nucl. Phys. **A656**, 3 (1999).
[10] F. Ajzenberg-Selove, Nucl. Phys. **A190**, 3 (1972).
[11] D.R. Tilley, H.R. Weller, C.M. Cheves, and R.M. Chasteler, Nucl. Phys. **A595**, 1 (1995).
[12] P.D. Parker, Phys. Rev. **173**, 1021 (1968).
[13] J.F. Ziegler, *Helium Stopping Powers and Ranges in All Elements* (Pergamon, New York, 1977).
[14] C. Rolfs, A.M. Charlesworth, and R.E. Azuma, Nucl. Phys. **A199**, 257 (1973).
[15] P.M. Endt, Nucl. Phys. **A521**, 1 (1990).
[16] C. Rolfs, Nucl. Phys. **A217**, 29 (1973).
[17] U. Schröder *et al.*, Nucl. Phys. **A467**, 240 (1987).
[18] R. Brun and F. Carminati, GEANT Detector Description and Simulation Tool, CERN Program Library Long Writeup W5013 edition, CERN, Geneva 1993, Switzerland.
[19] G. Audi and A.H. Wapstra, Nucl. Phys. **A595**, 409 (1995).
[20] C. Rolfs, I. Berka, and R.E. Azuma, Nucl. Phys. **A199**, 306 (1973).
[21] A. Cunsolo, A. Foti, G. Imme, P. Pappalardo, G. Raciti, N. Saunier, Phys. Rev. C **24**, 476 (1981).
[22] J.F. Wilkerson, R.E. Anderson, T.B. Clegg, E.J. Ludwig, and W.J. Thompson, Phys. Rev. Lett. **51**, 2269 (1983).
[23] A. Bohr and B. Mottelson, *Nuclear Structure* (Benjamin, Reading, MA, 1975).
[24] E. Anders and M. Grevesse, Geochim. Cosmochim. Acta **53**, 197 (1989).
[25] U. Giesen, C.P. Browne, J. Görres, J.G. Ross, M. Wiescher, R.E. Azuma, J.D. King, J.B. Vise, and M. Buckby, Nucl. Phys. **A567**, 146 (1994).